

# A Spacetime Calculation of the Calabrese-Cardy Entanglement Entropy

Abhishek Mathur\*, Sumati Surya and Nomaan X

*Raman Research Institute, CV Raman Ave, Sadashivanagar, Bangalore, 560080, India*

## Abstract

We calculate Sorkin’s spacetime entanglement entropy of a Gaussian scalar field for complementary regions in the 2d cylinder spacetime and show that it has the Calabrese-Cardy form. We find that the cut-off dependent term is universal when we use a covariant UV cut-off as in [1]. In addition, we show that the relative size-dependent term exhibits complementarity. Its coefficient is however *not* universal and depends on the choice of pure state. It asymptotes to the universal form within a natural class of pure states.

The Calabrese-Cardy formula for the entanglement entropy (EE) of a CFT for an interval  $\mathcal{I}_s$  of length  $s$  in a circle  $\mathcal{C}_\ell$  of circumference  $\ell$  is given by

$$S = \frac{c}{3} \ln \left( \frac{\ell}{\pi\epsilon} \right) + \frac{c}{3} \ln(\sin(\alpha\pi)) + c_1 \quad (1)$$

where  $\alpha = s/\ell$ ,  $c$  is the CFT central charge,  $\epsilon$  is a UV cut-off and  $c_1$  is a non-universal constant [2]. This formula has been shown to apply to a diverse range of two dimensional systems which fall within the same universality class, including a geometric realisation by Ryu and Takayanagi [3] and others [4]. Entanglement entropy (EE) was first proposed in [5] as a possible contributor to black hole entropy. Hence understanding Eqn. (1) from a spacetime perspective is of broad interest.

As a follow up to their earlier work, Calabrese and Cardy studied the unitary time evolution of the EE for an interval  $\mathcal{I}_s$  inside a larger interval  $\mathcal{I} \supset \mathcal{I}_s$ . Starting with a pure state, which is an eigenstate of a ”pre-quench” Hamiltonian, and then quenching the system at  $t = 0$ , they used path integral techniques to show that the EE increases with time. It then saturates after the ”light-crossing” time, in keeping with causality [6]. This corresponds to the ”time” required for the domain of dependence of  $\mathcal{I}_s$  to be fully defined. Seeking out a covariant formulation of EE is therefore of interest both to understanding the results of [6]

---

\**abhishekmathur@rri.res.in*

in a spacetime language as well as more generally in QFT and quantum gravity. Such a formulation is moreover in keeping with the broader framework of AQFT, where observables are associated with spacetime regions rather than spatial hypersurfaces [7].

In [8] Sorkin proposed a spacetime formula for the EE of a Gaussian scalar field  $\Phi$  in a globally hyperbolic subregion  $\mathcal{O}$  of a globally hyperbolic spacetime  $(M, g)$ , with respect to its causal complement  $\mathcal{O}^c$ . It uses the restriction of the Wightmann function  $W(x, x')$  in  $M$  to  $\mathcal{O}$ , and the Pauli-Jordan function  $i\Delta(x, x')$  which appears in the Peierl's spacetime commutation relation  $[\hat{\Phi}(x), \hat{\Phi}(x')] = i\Delta(x, x')$ .

Sorkin's spacetime EE (SSEE) of  $\mathcal{O}$  with respect to  $\mathcal{O}^c$  is

$$\mathcal{S} = \sum_{\mu} \mu \ln(|\mu|), \quad \widehat{W}|_{\mathcal{O}} \circ \chi = \mu(i\widehat{\Delta}) \circ \chi, \quad (2)$$

where  $\chi \notin \text{Ker}(\widehat{\Delta})$  and where

$$A \circ v(x) \equiv \int_{\mathcal{O}} dV_{x'} A(x, x') v(x'). \quad (3)$$

It is motivated by the finite system Wightmann function for a Gaussian state which is a direct sum of identical systems with two degrees of freedom [8]. The SSEE formula generalises the calculation of EE for a state at a given time to that associated with a spacetime region.

In [1] the SSEE for nested causal diamonds  $\mathcal{D}_s \subset \mathcal{D}_S$  was shown to yield the first, cut-off dependent term of Eqn. (1) with  $c = 1$  when  $s \ll S$ . Since  $\mathcal{D}_s$  is the domain of dependence of  $\mathcal{I}_s$ , this is the natural spacetime analogue of  $\mathcal{I}_s \subset \mathcal{I}_S$ . In this work we calculate the SSEE for the spacetime analogue of  $\mathcal{I}_s \subset \mathcal{C}_\ell$  for finite  $\ell$  and additionally, find the same  $\alpha$ -dependence as Eqn. (1), thus explicitly demonstrating complementarity. A natural spacetime analogue of  $\mathcal{C}_\ell$  is its (zero momentum) Cauchy completion, which is the  $d = 2$  cylindrical spacetime  $(M, g)$  with  $ds^2 = -dt^2 + dx^2$ ,  $x + \ell \sim x$ . The domains of dependence of  $\mathcal{I}_s$  and its complement  $\mathcal{I}_{\ell-s}$  in  $(M, g)$  are the causal diamonds  $\mathcal{D}_s$  and  $\mathcal{D}_{\ell-s}$  respectively, as shown in Fig 1.

In what follows we use a mixture of analytical and numerical methods to solve the SSEE eigenvalue problem.

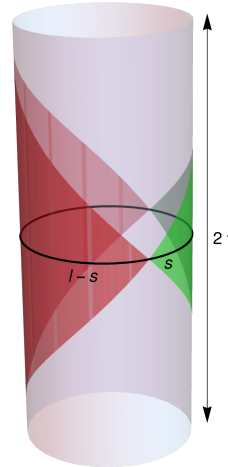


Figure 1: The spacetime analogues of  $\mathcal{I}_s, \mathcal{I}_{\ell-s} \subset \mathcal{C}_\ell$  are their domains of dependence  $\mathcal{D}_s$  and  $\mathcal{D}_{\ell-s}$  in  $(M, g)$  shown in green and red respectively.

We will find it convenient to work with the Sorkin-Johnston (SJ) formulation [9, 10, 11, 12, 13], where the SJ spectrum provides the required (covariant) UV cut-off with which to calculate  $\mathcal{S}$ , as was done in [1]. For a compact globally hyperbolic region  $(M, g)$  of a spacetime it follows from  $\text{Ker}(\widehat{\square}) = \text{Im}(i\widehat{\Delta})$  [14] that the eigenmodes of the integral Hermitian operator  $i\widehat{\Delta}$  provide a covariant orthonormal basis (the SJ modes) with respect to the  $\mathcal{L}^2$  norm on  $(M, g)$  [7]. The SJ vacuum or Wightmann function is given by the positive part of  $i\widehat{\Delta}$ . Since the SJ spectrum is covariant so is a UV cut-off in this basis.

For our calculation of  $\mathcal{S}$  we will use the SJ vacuum  $W_\tau$  for a free massless scalar field in a slab  $(M_\tau, g)$  of height  $2\tau$  in the cylinder spacetime [10], and its restriction to  $\mathcal{D}_s \subset M_\tau$ ,

$$W_\tau(x, t; x', t') = \sum_{m \in \mathbb{Z}} \varrho_m \psi_m(x, t) \psi_m^*(x', t'), \quad (4)$$

where  $\{\psi_m, \varrho_m\}$  are the  $\mathcal{L}^2$  normalised positive frequency SJ eigenmodes and eigenvalues in  $M_\tau$  [10]:

$$\begin{aligned} \psi_m(x, t) &= \left( \frac{(1 - \zeta_m)}{2\sqrt{2\ell c_m}} e^{i2\pi|m|t/\ell} + \frac{(1 + \zeta_m)}{2\sqrt{2\ell c_m}} e^{-i2\pi|m|t/\ell} \right) e^{i2\pi mx/\ell} \\ \varrho_m &= \ell \frac{s_m c_m}{2\pi|m|}, \quad \zeta_m = \frac{c_m}{s_m}, \quad \gamma = \frac{2\tau}{\ell}, \quad m \in \mathbb{Z}, \\ c_m^2 &= \tau (1 + \text{sinc}(2|m|\pi\gamma)), \quad s_m^2 = \tau (1 - \text{sinc}(2|m|\pi\gamma)). \end{aligned} \quad (5)$$

The  $m = 0$  “zero mode” in particular takes the form

$$\psi_0(t) = \frac{1}{2\sqrt{\tau\ell}} \left( 1 - i \frac{\sqrt{3}}{\tau} t \right), \quad \varrho_0 = \frac{2}{\sqrt{3}} \tau^2. \quad (6)$$

Unlike the standard vacuum on the cylinder,  $W_\tau$  is  $\tau$ -dependent. Each  $W_\tau$  can however be viewed as a pure (non-vacuum) state in  $M_{\bar{\tau}}$  for any  $\bar{\tau} > \tau$ , as we will later show. To accommodate both  $\mathcal{D}_s$  and  $\mathcal{D}_{\ell-s}$  in our calculations, we require  $2\tau \geq s, \ell - s$ .

The SJ modes in  $\mathcal{D}_s$  are naturally expressed in terms of the light cone coordinates  $u = \frac{1}{\sqrt{2}}(t - x), v = \frac{1}{\sqrt{2}}(t + x)$  and come in the two mutually orthogonal series [15]

$$\begin{aligned} f_k &= e^{-iku} - e^{-ikv}, \quad k = 2\sqrt{2}n\pi/s \\ g_\kappa &= e^{-i\kappa u} + e^{-i\kappa v} - 2 \cos\left(\frac{\kappa s}{2\sqrt{2}}\right), \quad \tan\left(\frac{\kappa s}{2\sqrt{2}}\right) = \frac{\kappa s}{\sqrt{2}} \end{aligned} \quad (7)$$

with eigenvalues  $\lambda_k = \frac{s}{2\sqrt{2}k}$  and  $\lambda_\kappa = \frac{s}{2\sqrt{2}\kappa}$ , respectively, and with  $\mathcal{L}^2$  norm in  $\mathcal{D}_s$

$$\|f_k\|^2 = s^2, \quad \|g_\kappa\|^2 = s^2 \left( 1 - 2 \cos^2\left(\frac{\kappa s}{2\sqrt{2}}\right) \right). \quad (8)$$

Since  $i\widehat{\Delta}$  is diagonal in this basis we will use it to transform Eqn. (2) to the matrix form

$$\widehat{W}_\tau|_{\mathcal{D}_s}X = \mu\Lambda X, \quad (9)$$

where  $\Lambda$  is the diagonal matrix  $\{\lambda_k, \lambda_\kappa\}$ . For  $X \notin \text{Ker}(i\widehat{\Delta})$ , we can invert this to suggestively write

$$\widehat{\rho}X = \Lambda^{-1}\widehat{W}_\tau|_{\mathcal{D}_s}X = \mu X, \quad (10)$$

so that  $\mathcal{S}$  can be viewed as the von-Neumann entropy of  $\widehat{\rho}$ . The spectrum of  $\widehat{\rho}$  is unbounded and hence needs a UV cut-off. As in [1] we use the covariant UV-cut off with respect to the SJ spectrum  $\{\lambda_k, \lambda_\kappa\}$ . For large  $\kappa$  the condition  $\tan(\kappa s/2\sqrt{2}) = \kappa s/\sqrt{2}$  can be approximated by  $\kappa \sim \sqrt{2}(2n+1)\pi/s$ , so that a consistent choice of cut-off for both sets of eigenvalues is  $\epsilon = k_{\max}^{-1} = s/(2\sqrt{2}n_{\max}\pi)$ . We also need to ensure that this same cut-off is used in the causal complement, i.e.,  $k_{\max} = 2\sqrt{2}n'_{\max}\pi/(\ell - s)$ , where  $n'$  denotes the quantum number for the SJ spectrum in  $\mathcal{D}_{\ell-s}$ , so that  $\epsilon = \frac{\ell\alpha}{2\sqrt{2}\pi n_{\max}} = \frac{\ell(1-\alpha)}{2\sqrt{2}\pi n'_{\max}}$ .

We expand the SJ modes in  $M_\tau$  in terms of those in  $\mathcal{D}_s$  to obtain the non-zero matrix elements for  $\widehat{W}_\tau|_{\mathcal{D}_s}$  for general  $\alpha, \gamma$ . Suppressing the  $\tau, \mathcal{D}_s$  labels, these are

$$\begin{aligned} \widehat{W}_{kk'} &= \frac{s^4}{32\pi} \sum_{m>0} \frac{1}{|m|\zeta_m} \left( \eta_m^- \text{sinc}(x_+) - \eta_m^+ \text{sinc}(x_-) \right) \times \left( \eta_m^- \text{sinc}(x'_+) - \eta_m^+ \text{sinc}(x'_-) \right) \\ \widehat{W}_{\kappa\kappa'} &= \frac{s^4}{32\pi} \sum_{m>0} \frac{1}{|m|\zeta_m} \left( \eta_m^- \text{sinc}(z_+) + \eta_m^+ \text{sinc}(z_-) \right) \times \left( \eta_m^- \text{sinc}(z'_+) + \eta_m^+ \text{sinc}(z'_-) \right) \\ &\quad + \widehat{W}_{\kappa\kappa'}^{(0)} \end{aligned} \quad (11)$$

where  $x_\pm = (n \pm \alpha m)\pi$ ,  $x'_\pm = (n' \pm \alpha m)\pi$ ,  $z_\pm = \kappa s/2\sqrt{2} \pm \alpha m\pi$ ,  $z'_\pm = \kappa' s/2\sqrt{2} \pm \alpha m\pi$ , and the contribution from the zero mode is

$$\begin{aligned} \widehat{W}_{\kappa\kappa'}^{(0)} &= \frac{s^4}{2\sqrt{3}} \frac{\tau}{\ell} \cos(\kappa s/(2\sqrt{2})) \cos(\kappa' s/(2\sqrt{2})) \\ &\quad \times \left( 1 + \sqrt{\frac{3}{2}} \frac{1}{\kappa\tau} \right) \left( 1 + \sqrt{\frac{3}{2}} \frac{1}{\kappa'\tau} \right). \end{aligned} \quad (12)$$

Our strategy is to construct  $\widehat{\rho}$  from these matrix elements and to solve for its eigenvalues using a numerical matrix solver. However, each matrix elements in Eqn. (11) is an infinite sum over the quantum number  $m$  and hence not amenable to explicit calculation. We therefore need to find a closed form expression for the above matrix elements.

We notice that when  $\gamma$  takes half-integer values (for which the SJ vacuum Hadamard [10]),  $\zeta_m = 1$  for  $m \neq 0$ , which leads to a considerable simplification. Further, let  $\alpha$  be rational, so that we can write  $\alpha = \frac{p}{q}$ , with  $p, q \in \mathbb{Z}$ , and  $p, q > 0$  being relatively prime. For these choices of  $\alpha$  and  $\gamma$ , the infinite sums of Eqn. (11) reduce to the following finite sums over Polygamma functions  $\Psi(x)$  and  $\Psi^{(1)}(x)$

$$\begin{aligned}
\widehat{W}_{kk'} &= \frac{s^4}{8\pi n} \left[ \delta_{n,n'} \left( \alpha \Theta(n) \sum_m \delta_{n,m\alpha} + \frac{1}{\pi^2 \alpha q^2 n} \sum_{r=1}^{q-1} \sin^2(r\alpha\pi) \left[ -\alpha q \Psi\left(\frac{r}{q}\right) + \alpha q \Psi\left(\frac{\alpha r - n}{\alpha q}\right) \right. \right. \right. \\
&\quad \left. \left. \left. + n \Psi^{(1)}\left(\frac{\alpha r - n}{\alpha q}\right) \right] \right) + (1 - \delta_{n,n'}) \frac{(-1)^{n+n'}}{\pi^2 n'(n-n')q} \sum_{r=1}^{q-1} \sin^2(r\alpha\pi) \left[ (n' - n) \Psi\left(\frac{r}{q}\right) \right. \right. \\
&\quad \left. \left. - n' \Psi\left(\frac{\alpha r - n}{\alpha q}\right) + n \Psi\left(\frac{\alpha r - n'}{\alpha q}\right) \right] \right] \\
\widehat{W}_{\kappa\kappa'} &= s^4 \cos\left(\frac{\kappa s}{2\sqrt{2}}\right) \cos\left(\frac{\kappa' s}{2\sqrt{2}}\right) \left[ \frac{\tau}{2\sqrt{3}\ell} \left(1 + \sqrt{\frac{3}{2}} \frac{1}{\tau\kappa}\right) \left(1 + \sqrt{\frac{3}{2}} \frac{1}{\tau\kappa'}\right) \right. \\
&\quad \left. + \delta_{\kappa,\kappa'} \frac{1}{\alpha q^2 s^2 \kappa^2 \pi^2} \left( \sum_{r=1}^{q-1} \Omega(\kappa, \kappa', \alpha, r) \left[ \alpha q \pi \left( \Psi\left(\frac{r}{q} - \frac{\kappa s}{\eta}\right) - \Psi\left(\frac{r}{q}\right) \right) + \frac{\kappa s}{2\sqrt{2}} \Psi^{(1)}\left(\frac{r}{q} - \frac{\kappa s}{\eta}\right) \right] \right. \right. \\
&\quad \left. \left. + \frac{s^2 \kappa \kappa'}{2} \left[ \alpha q \pi \left( \gamma_e + \Psi\left(1 - \frac{\kappa s}{\eta}\right) \right) + \frac{\kappa s}{2\sqrt{2}} \Psi^{(1)}\left(1 - \frac{\kappa s}{\eta}\right) \right] \right) + (1 - \delta_{\kappa,\kappa'}) \frac{1}{s^2 q \kappa \kappa' (\kappa - \kappa')} \right. \\
&\quad \times \left( \sum_{r=1}^{q-1} \Omega(\kappa, \kappa', \alpha, r) \left[ \kappa \Psi\left(\frac{r}{q} - \frac{\kappa' s}{\eta}\right) - \kappa' \Psi\left(\frac{r}{q} - \frac{\kappa s}{\eta}\right) - (\kappa - \kappa') \Psi\left(\frac{r}{q}\right) \right] \right. \\
&\quad \left. \left. + \frac{s^2 \kappa \kappa'}{2} \left[ \gamma_e (\kappa - \kappa') + \kappa \Psi\left(1 - \frac{\kappa' s}{\eta}\right) - \kappa' \Psi\left(1 - \frac{\kappa s}{\eta}\right) \right] \right) \right], \quad \eta = 2\sqrt{2}\alpha q \pi \quad (13)
\end{aligned}$$

where  $\gamma_e$  represents the Euler-Mascheroni constant and

$$\begin{aligned}
\Omega(\kappa, \kappa', \alpha, r) &= \kappa \kappa' \frac{s^2}{2} \cos^2(\alpha r \pi) + \sin^2(\alpha r \pi) \\
&\quad - (\kappa + \kappa') \frac{s}{2\sqrt{2}} \sin(2\alpha r \pi). \quad (14)
\end{aligned}$$

We are now in a position to solve for the eigenvalues of  $\widehat{\rho}$  using Mathematica's numerical eigenvalue solver. We consider a range of values of  $\alpha, \gamma$  and the cut-off  $n_{\max}/\alpha$  given in the table below.

$\alpha$	$\frac{1}{10}, \frac{1}{5}, \frac{1}{4}, \frac{1}{3}, \frac{1}{2}, \frac{2}{3}, \frac{3}{4}, \frac{4}{5}, \frac{9}{10}$
$\gamma$	1, 2, 4, 6, 8, 16, 21.5, 32, 40.3, 100, 200, 1000, 2000
$\frac{n_{\max}}{\alpha}$	1000, 1200, 1400, 1600, 1800, 2000, 2200, 2400, 2600

In the list of  $\gamma$  values, we have also included the specific non-half-integer value of  $\gamma = 40.3$  for which  $\zeta_m \sim 1$  even for  $m = 1$ . In general, we note that  $\zeta_m \sim 1$  for  $m \gg \gamma^{-1}$ . The

error coming from small  $m$  terms has been explicitly calculated in this case as a function of  $m$  and seen to be small. For the special case  $\alpha = 0$ ,  $\mathcal{S}$  is trivially zero, while for  $\alpha = 1$ , the domain of dependence of  $\mathcal{C}_\ell$  is no longer a causal diamond, but all of  $M_\tau$ . Since  $\widehat{W}_\tau$  is the SJ vacuum and therefore pure,  $\mathcal{S} = 0$ .

Fig. 2 shows the results of simulations for these various  $\alpha$  and  $\gamma$  values, for a fixed choice of cut-off  $n_{\max}/\alpha = 2600$ . It is already clear that  $\mathcal{S}$  satisfies complementarity. This is much more explicit in Fig. 3, where we vary over the cut-off. Our numerical results suggest that

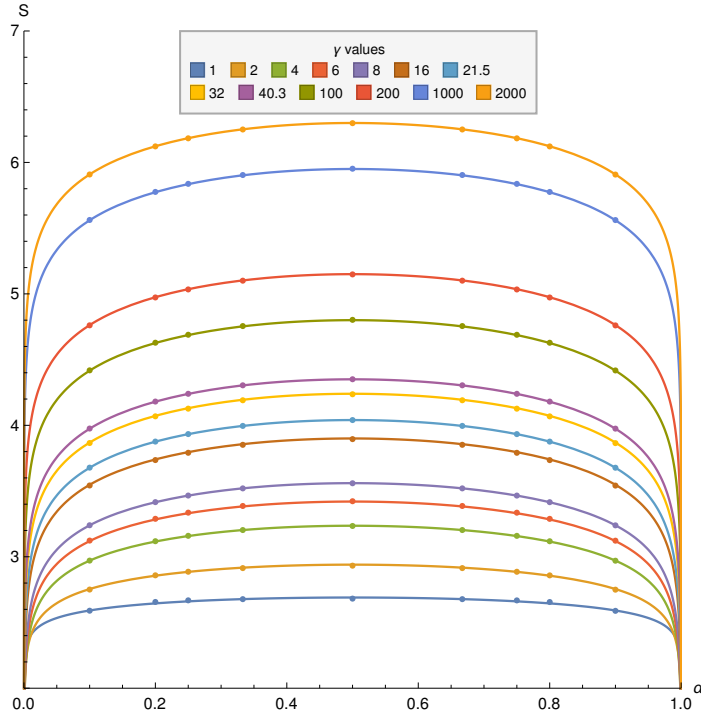


Figure 2:  $\mathcal{S}$  vs  $\alpha$  for different  $\gamma$  fitted to  $\mathcal{S} = a \log(\sin(\pi\alpha)) + b$ , with  $\frac{n_{\max}}{\alpha} = 2600$ .

$\mathcal{S}$  takes the general form

$$\mathcal{S} = \frac{c(\gamma)}{3} \ln\left(\frac{\ell}{\pi\epsilon}\right) + f(\gamma) \ln(\sin(\alpha\pi)) + c_1(\gamma). \quad (15)$$

Using the best-fit curves in Figs. 3-5, and the associated data in the appendix, we find that  $c(\gamma) \sim 1$  and

$$\begin{aligned} f(\gamma) &\sim 0.33 + a/\gamma + b/\gamma^2 \\ c_1(\gamma) &\sim a' \log \gamma + b'. \end{aligned} \quad (16)$$

Thus, the first term of Eqn. (1) is reproduced for any choice of  $\alpha, \gamma$ . This generalises the results of [1] where this was shown in the limit of  $\alpha \ll 1$ . The dependence on  $\alpha$ , i.e.,

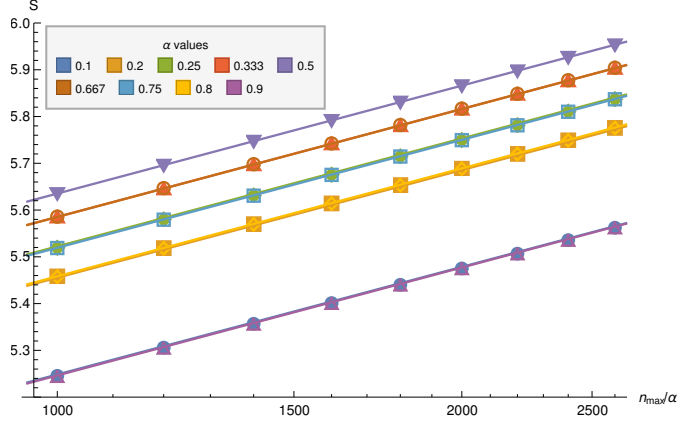


Figure 3: Log-linear plot of  $\mathcal{S}$  vs  $\frac{n_{\max}}{\alpha}$  for different  $\alpha$  fitted to  $\mathcal{S} = a \log(n_{\max}/\alpha) + b$  for  $\gamma = 1000$ .

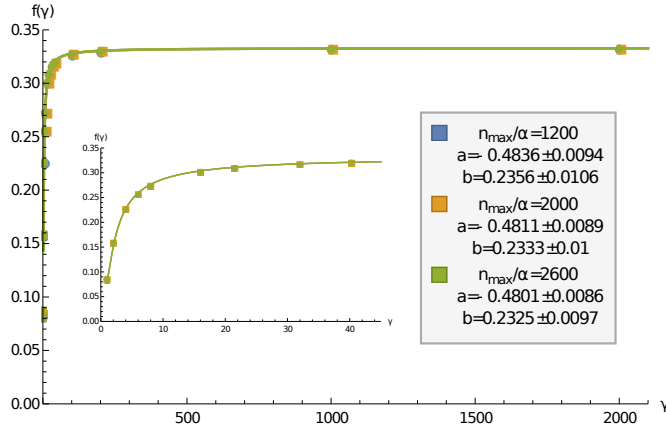


Figure 4: A plot of  $f(\gamma)$  vs.  $\gamma$  for different values of  $n_{\max}/\alpha$ , fitted to  $0.33 + a/\gamma + b/\gamma^2$ . The inset figure shows the smaller  $\gamma$  values.

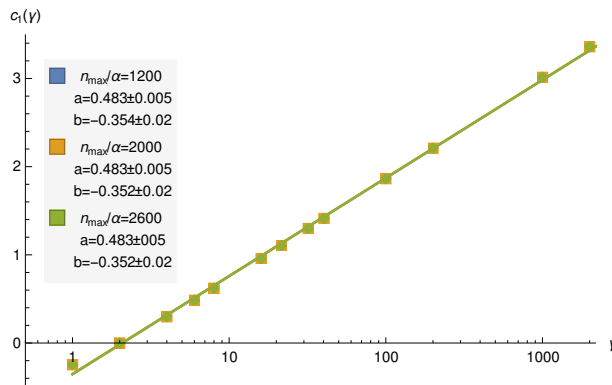


Figure 5: A log-linear plot of  $c_1(\gamma)$  vs  $\gamma$  for different values of  $n_{\max}/\alpha$  fitted to  $a \log \gamma + b$ .

the second term of Eqn. (1) is also reproduced and hence exhibits complementarity for any  $\alpha$  (see Fig. 2, 3). Its coefficient however is *not* universal and depends on  $\gamma$  as shown in Fig. 4. However, as  $\gamma \gg 1$ ,  $f(\gamma)$  does asymptote to the universal value  $1/3$ . Finally, the non-universal constant  $c_1(\gamma)$  diverges logarithmically with  $\gamma$  as shown in Fig. 5. This can be traced to the IR divergence in the zero modes of the massless theory.

The behaviour of  $f(\gamma)$  can be viewed as a dependence on the choice of the pure state  $W_\tau$  in  $M_{\bar{\tau}}$ , for  $M_{\bar{\tau}} \supset M_\tau$ . From Eqn. (4) we see that  $\widehat{W}_\tau$  is a state in  $M_{\bar{\tau}}$ , i.e.,  $\widehat{W}_\tau = \widehat{R}_\tau + i\widehat{\Delta}/2$ , where  $\widehat{R}_\tau$  is real and symmetric.

Expanding  $i\widehat{\Delta}$  in the SJ modes  $\{\psi_m^{(\bar{\tau})}\}$  of  $M_{\bar{\tau}}$  and  $\widehat{W}_\tau$  in  $\{\psi_m^{(\tau)}\}$ , and inserting in Eqn. (2) we see that term by term

$$\varrho_m^\tau \psi_m^{(\tau)}(x, t) A_m = \mu \varrho_m^{\bar{\tau}} [\psi_m^{(\bar{\tau})}(t, x) \bar{A}_m - \psi_m^{*(\bar{\tau})}(t, x) \bar{B}_m],$$

where  $A_m = (\psi_m^{(\tau)}, \chi)_{\bar{\tau}}$ ,  $\bar{A}_m = (\psi_m^{(\bar{\tau})}, \chi)_{\bar{\tau}}$ ,  $\bar{B}_m = (\psi_m^{*(\bar{\tau})}, \chi)_{\bar{\tau}}$  and  $(\cdot, \cdot)_{\bar{\tau}}$  is the  $\mathcal{L}^2$  inner product in  $M_{\bar{\tau}}$ . Expanding  $\psi_m^{(\tau)} = a_m \psi_m^{(\bar{\tau})} + b_m \psi_m^{*(\bar{\tau})}$ ,  $a_m = \frac{s_m^{\tau'}}{2c_m^{\tau'}} (\zeta_m^{(\tau')} + \zeta_m^{(\tau)})$ ,  $b_m = \frac{s_m^{\tau'}}{2c_m^{\tau'}} (\zeta_m^{(\tau')} - \zeta_m^{(\tau)})$  this simplifies to

$$\begin{aligned} \varrho_m^\tau a_m (a_m \bar{A}_m + b_m \bar{B}_m) &= \mu \varrho_m^{\bar{\tau}} \bar{A}_m \\ \varrho_m^\tau b_m (a_m \bar{A}_m + b_m \bar{B}_m) &= -\mu \varrho_m^{\bar{\tau}} \bar{B}_m. \end{aligned} \quad (17)$$

The solutions for this are either  $a_m \bar{A}_m + b_m \bar{B}_m = 0 \Rightarrow \mu = 0$ , or  $a_m \bar{B}_m + b_m \bar{A}_m = 0 \Rightarrow \mu = \frac{\varrho_m^\tau}{\varrho_m^{\bar{\tau}}} (a_m^2 - b_m^2) = 1$ , which means that  $\widehat{W}_\tau$  is a pure state in  $M_{\bar{\tau}}$ . Thus  $f(\gamma)$  can be viewed as the dependence on the choice of pure state in  $M_{\bar{\tau}}$  for  $M_\tau \subset M_{\bar{\tau}}$ .

We end with some remarks. While we have demonstrated complementarity for certain rational values of  $\alpha$ , an analytic demonstration using Eqn. (13) seems non-trivial, in part because the UV regulated matrices  $\widehat{\rho}_\alpha$  and  $\widehat{\rho}_{1-\alpha}$  are of different dimensions. Conversely, complementarity implies that if  $n_{\max} > n'_{\max}$ ,  $\widehat{\rho}_\alpha = \widehat{\rho}_{1-\alpha} \oplus \mathbf{1}_N \oplus \mathbf{0}_N$ , where  $\mathbf{0}$  is the zero matrix and  $N = (n_{\max} - n'_{\max})/2$ .

In our computations we find that the eigenvalues of  $\widehat{\rho}$  (which always come in pairs  $(\mu, 1 - \mu)$ ) exhibit the surprising feature that all but one pair hovers around the values 0 and 1, thus contributing most significantly to  $\mathcal{S}$ . Indeed, the  $\mathcal{S}$  calculated using the largest few pairs of eigenvalues accounts for most of the entropy (see appendix).

Finally, it would be interesting to calculate the non-zero mass case which is IR divergence free. While the small mass approximation of the SJ modes in  $\mathcal{D}_s$  is known [16], the challenge will be to obtain closed form expressions for the matrix elements of  $\widehat{W}$  as we have done.

## Acknowledgements

SS is supported in part by a Visiting Fellowship at the Perimeter Institute. Research at Perimeter Institute is supported in part by the Government of Canada through the Depart-



ment of Innovation, Science and Economic Development Canada and by the Province of Ontario through the Ministry of Colleges and Universities.

## Appendix: Supporting Data

In this appendix we present some plots with additional data which were used to compute the coefficients  $c(\gamma)$ ,  $f(\gamma)$  and  $c_1(\gamma)$  in the Entanglement Entropy.

Fig. 6 shows the dependence of  $\mathcal{S}$  on  $\alpha$  for different values of  $\gamma$  and with three different values of  $n_{max}/\alpha$  (1200, 2000 and 2600). The SSEE can be fitted to the form  $\mathcal{S} = a_1 \log(\sin(\alpha\pi)) + b_1$  where the coefficient  $a_1$  corresponds to  $f(\gamma)$  in Eqn. (15). The values of  $a_1$  and  $b_1$  along with their errors are given in the tables in Fig. 6.  $a_1$  and therefore  $f(\gamma)$  can be seen to be independent of  $n_{max}/\alpha$ . It is however dependent on  $\gamma$  and asymptotes to the universal value of  $1/3$  in the Calabrese-Cardy formula for  $\gamma \gg 1$ . We fit  $f(\gamma)$  values to the form

$$f(\gamma) = 0.33 + a_2/\gamma + b_2/\gamma^2 \quad (18)$$

and find the  $a_2 \approx -0.48$  and  $b_2 \approx 0.23$  with the error given in the tables of Fig. 4.

Fig. 7 shows the dependence of  $\mathcal{S}$  on  $n_{max}/\alpha$  for different  $\alpha$  and with three different values of  $\gamma$  (16, 200 and 1000). Here SSEE can be fitted to the form,  $\mathcal{S} = a_3 \log(n_{max}/\alpha) + b_3$ . As is clear from the tables in this figure  $a_3 \approx 0.33 \approx 1/3$  for all  $\alpha$  and  $\gamma$  with the order of error given in the table.  $b_3$  however depends on  $\alpha$  and  $\gamma$ . This suggests that  $c(\gamma) \approx 1$  in Eqn. (15).

In order to extract  $c_1(\gamma)$  we subtract the first term in Eqn. (15) (which depends on  $n_{max}/\alpha$ ) using  $c(\gamma)/3$  given by the values of  $a_3$  in the table of Fig. 7 from the values of  $b_1$  in the table of Fig. 6 for  $n_{max}/\alpha = 1200, 2000$  and  $2600$ . We find that the difference (or  $c_1(\gamma)$ ) is independent of the choice of  $n_{max}/\alpha$  which is as expected. We fit the dependence on  $\gamma$  by

$$c_1(\gamma) = a_4 \log(\gamma) + b_4 \quad (19)$$

and the values for the coefficients are given in the table in the Fig. 5.

We also find that the eigenvalues (which always come in pairs  $(\mu, 1 - \mu)$ ) exhibit the surprising feature that all but one pair hovers around the values 0 and 1 and hence contributes significantly to  $\mathcal{S}$ . In Fig. 8 we also show the comparison of the eigenvalues obtained in the two complementary regions, we find that they differ only in the numbers of  $(0, 1)$  pairs. Further, if we calculate  $\mathcal{S}$  for the largest pairs of eigenvalues, we find that the error is small, as shown in Fig 9.

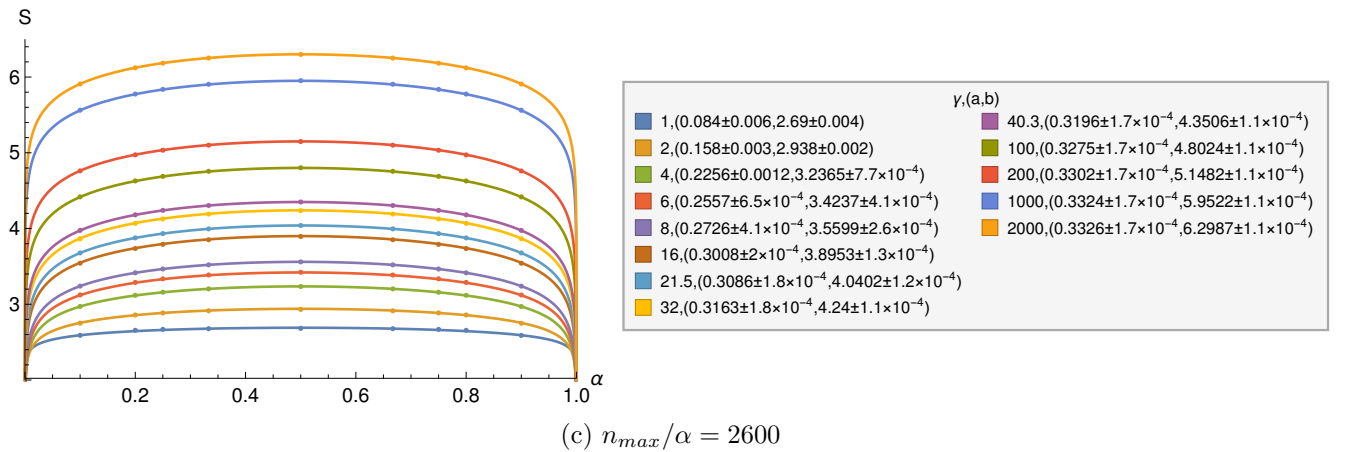
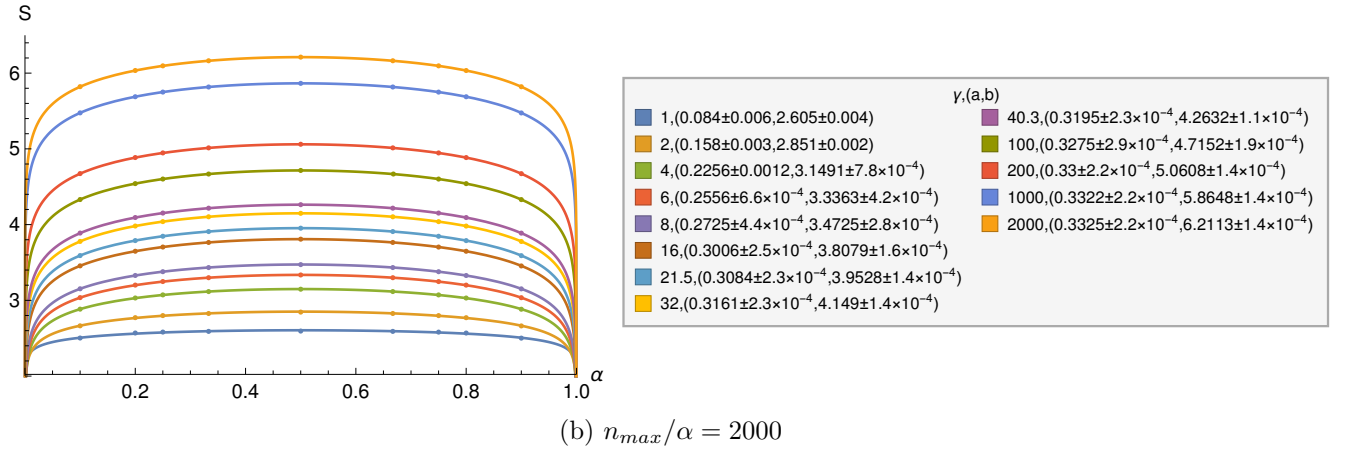
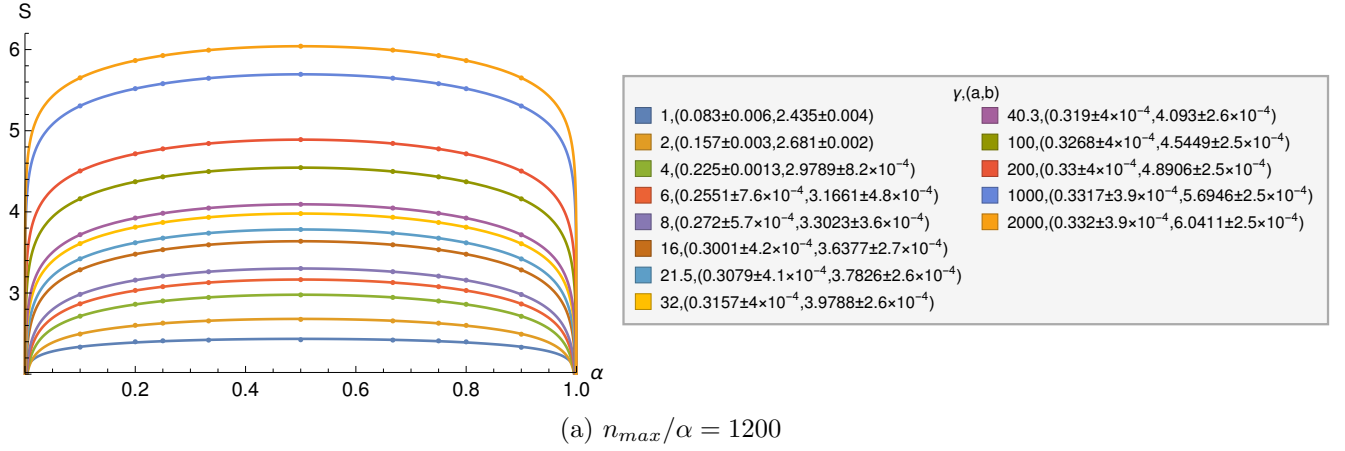


Figure 6:  $\mathcal{S}$  vs  $\alpha$  for different  $\gamma$  with  $n_{max}/\alpha = 1200, 2000$  and  $2600$  fitted to  $\mathcal{S} = a \log(\sin(\pi\alpha)) + b$ . The fit parameters are shown in the table.

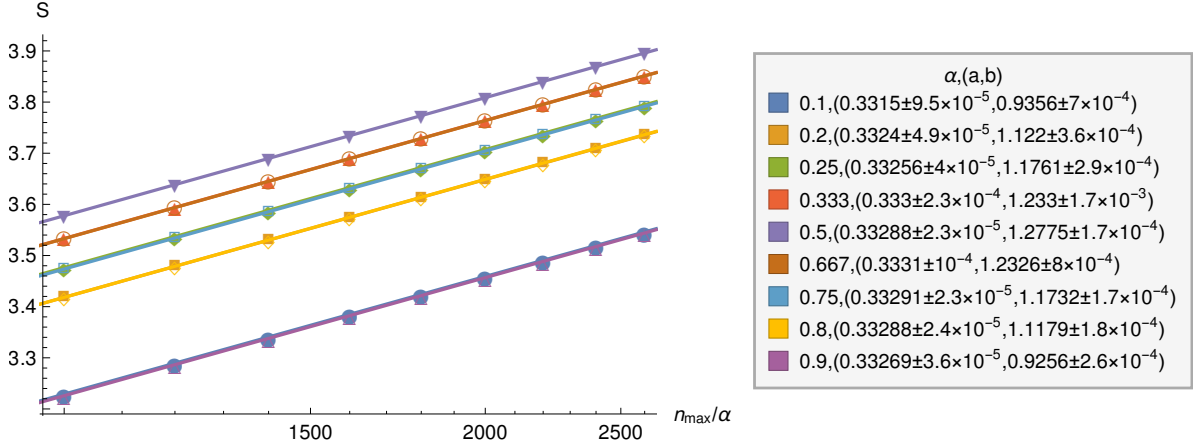
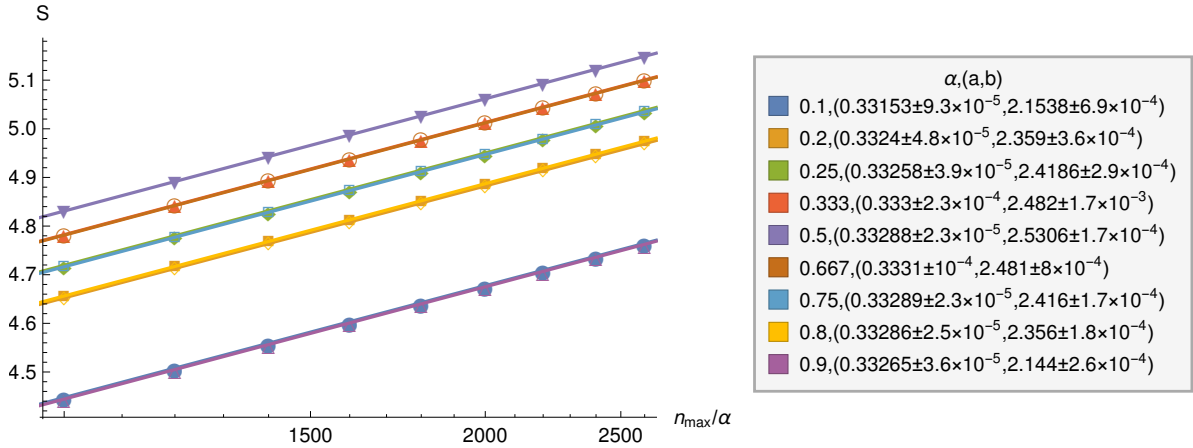
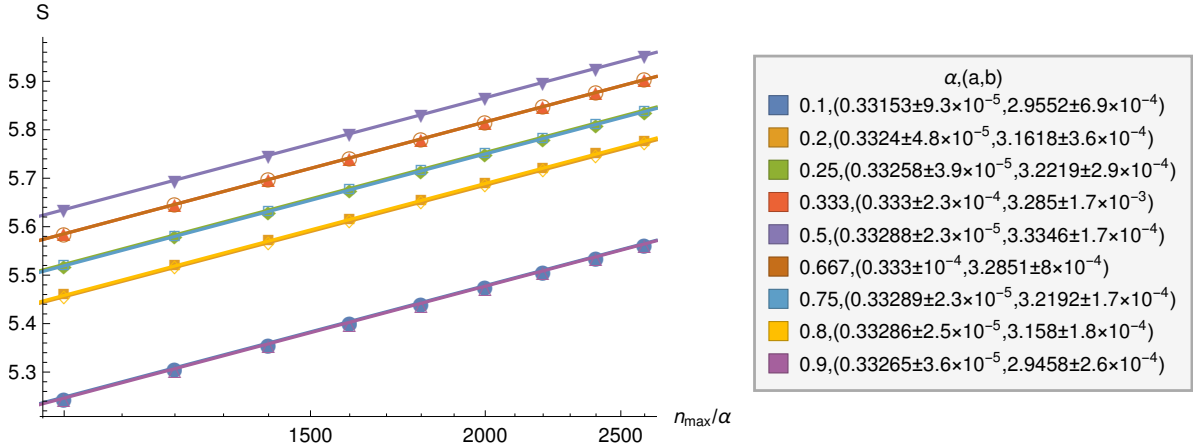
(a)  $\gamma = 16$ (b)  $\gamma = 200$ (c)  $\gamma = 1000$ 

Figure 7: A log-linear plot of  $\mathcal{S}$  vs  $n_{\max}/\alpha$  for different  $\alpha$  with  $\gamma = 16, 200$  and  $1000$  fitted to  $\mathcal{S} = a \log(n_{\max}/\alpha) + b$ . The fit parameters are shown in the table which show  $a \sim 1/3$ . This is also true for other values of  $\gamma$ . The curves for complementary values of  $\alpha$  are indistinguishable.

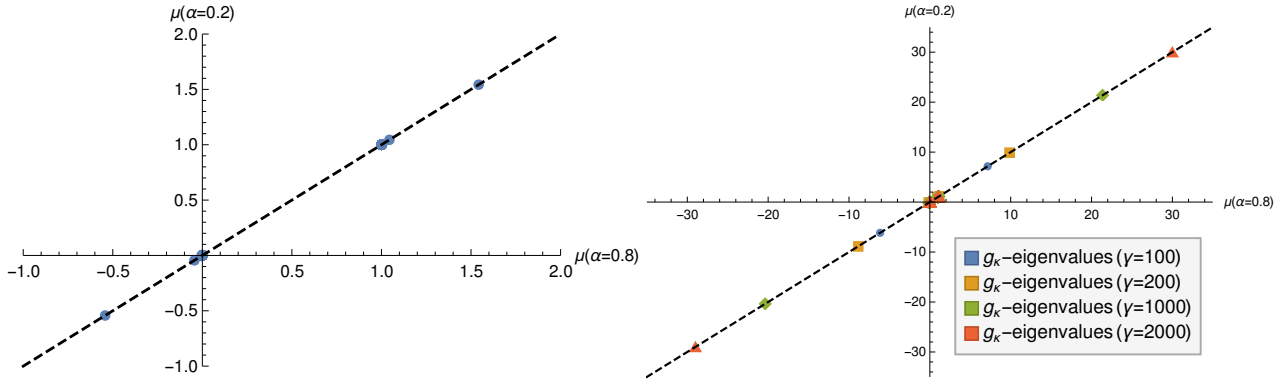


Figure 8: A plot comparing the eigenvalues  $\mu$  of the entropy equation for one choice of complementary regions with  $\alpha = 0.2, 0.8$  for  $n_{\max}/\alpha = 2600$  and different choices of  $\gamma$ . On the left are the eigenvalues associated with the  $f_k$  matrix elements which are independent of  $\gamma$  and on the right are those associated with the  $g_\kappa$ , which are  $\gamma$  dependent. We note that the number of eigenvalues differ in both regions but only in the number of  $(1, 0)$  pairs which leads to the equality of the SSEE in these complementary regions. Further, the significant contribution comes from the  $g_\kappa$  matrix elements of which there are precisely *two* which are substantially different from  $(1, 0)$ . These increase with  $\gamma$  and are the main contributors to  $c_1(\gamma)$

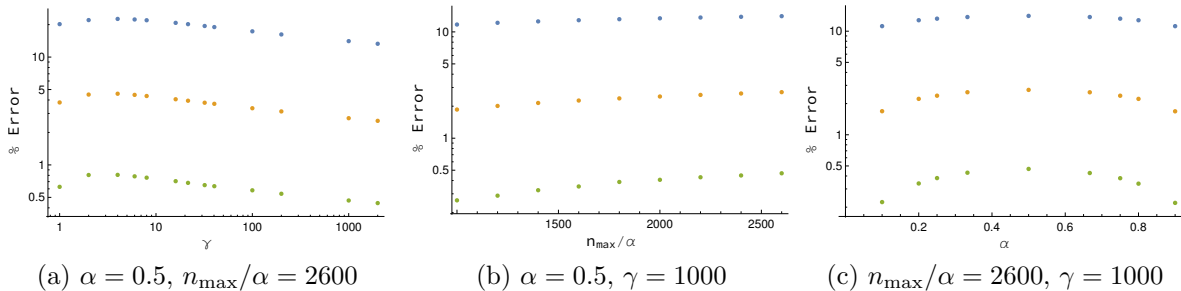


Figure 9: In order to estimate the contribution of the pairs  $(\mu, 1 - \mu)$ , we plot the percentage error in the SSEE when only the largest pairs (one, two and three represented in blue, orange and green respectively) of eigenvalues are considered, as a function of the different parameters  $\gamma, n_{\max}/\alpha$  and  $\alpha$ . In each case, we see that the error goes down to  $< 1\%$  even when only the 3 largest eigenvalues are retained.

## References

- [1] M. Saravani, R. D. Sorkin, and Y. K. Yazdi, “Spacetime entanglement entropy in  $1 + 1$  dimensions,” *Class. Quant. Grav.*, vol. 31, no. 21, p. 214006, 2014.
- [2] P. Calabrese and J. L. Cardy, “Entanglement entropy and quantum field theory,” *J. Stat. Mech.*, vol. 0406, p. P06002, 2004.

- [3] S. Ryu and T. Takayanagi, “Holographic derivation of entanglement entropy from the anti-de sitter space/conformal field theory correspondence,” *Physical review letters*, vol. 96, no. 18, p. 181602, 2006.
- [4] M. Headrick, “Lectures on entanglement entropy in field theory and holography,” *arXiv preprint arXiv:1907.08126*, 2019.
- [5] L. Bombelli, R. K. Koul, J. Lee, and R. D. Sorkin, “A Quantum Source of Entropy for Black Holes,” *Phys. Rev.*, vol. D34, pp. 373–383, 1986.
- [6] P. Calabrese and J. L. Cardy, “Evolution of entanglement entropy in one-dimensional systems,” *J. Stat. Mech.*, vol. 0504, p. P04010, 2005.
- [7] C. J. Fewster and K. Rejzner, “Algebraic quantum field theory,” in *Progress and Visions in Quantum Theory in View of Gravity*, pp. 1–61, Springer, 2020.
- [8] R. D. Sorkin, “Expressing entropy globally in terms of (4D) field-correlations,” *J. Phys. Conf. Ser.*, vol. 484, p. 012004, 2014.
- [9] R. D. Sorkin, “From Green Function to Quantum Field,” *Int. J. Geom. Meth. Mod. Phys.*, vol. 14, no. 08, p. 1740007, 2017.
- [10] C. J. Fewster and R. Verch, “On a Recent Construction of ‘Vacuum-like’ Quantum Field States in Curved Spacetime,” *Class. Quant. Grav.*, vol. 29, p. 205017, 2012.
- [11] M. Brum and K. Fredenhagen, “‘Vacuum-like’ Hadamard states for quantum fields on curved spacetimes,” *Class. Quant. Grav.*, vol. 31, p. 025024, 2014.
- [12] N. Afshordi, S. Aslanbeigi, and R. D. Sorkin, “A distinguished vacuum state for a quantum field in a curved spacetime: formalism, features, and cosmology,” *Journal of High Energy Physics*, vol. 2012, no. 8, p. 137, 2012.
- [13] N. Afshordi, M. Buck, F. Dowker, D. Rideout, R. D. Sorkin, and Y. K. Yazdi, “A Ground State for the Causal Diamond in 2 Dimensions,” *JHEP*, vol. 10, p. 088, 2012.
- [14] R. M. Wald, *Quantum field theory in curved spacetime and black hole thermodynamics*. University of Chicago press, 1994.
- [15] S. P. Johnston, *Quantum Fields on Causal Sets*. PhD thesis, Imperial Coll., London, 2010.
- [16] A. Mathur and S. Surya, “Sorkin-Johnston vacuum for a massive scalar field in the 2D causal diamond,” *Phys. Rev. D*, vol. 100, no. 4, p. 045007, 2019.